Electronic Supplementary Material (ESI) for Inorganic Chemistry Frontiers.
This journal is © The Partner Organisations 2020

Multi-functional Photoelectric Sensors based on A series of Isopolymolybdate-based Compounds for Detecting Different Ions

Chen Wang, Jun Ying*, Hai-chen Mou, Ai-xiang Tian, Xiu-li Wang*

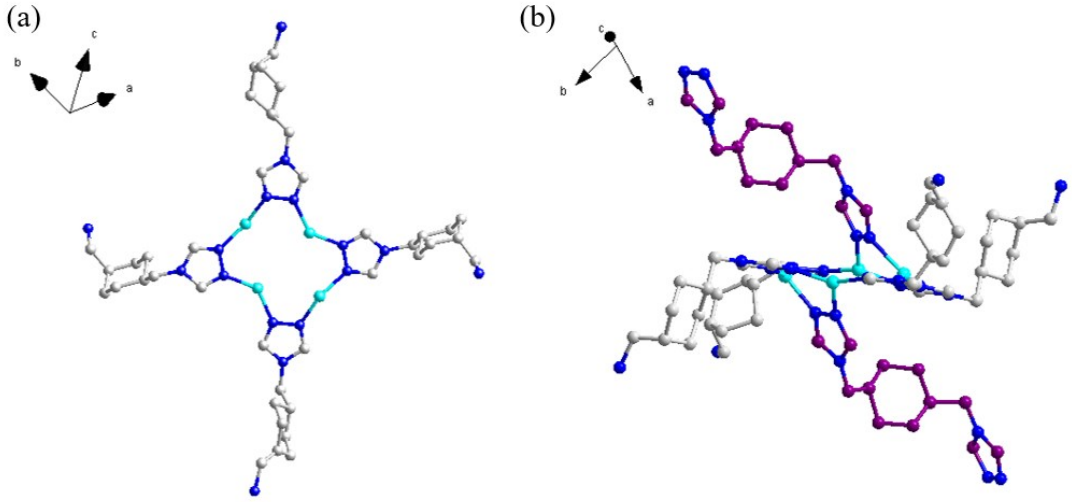

Fig. S1. (a) The tetranuclear copper cluster in compound **1** constructed by four ctcm molecules. (b) Two btmc ligands linking a tetranuclear copper cluster by Cu-N bonds.

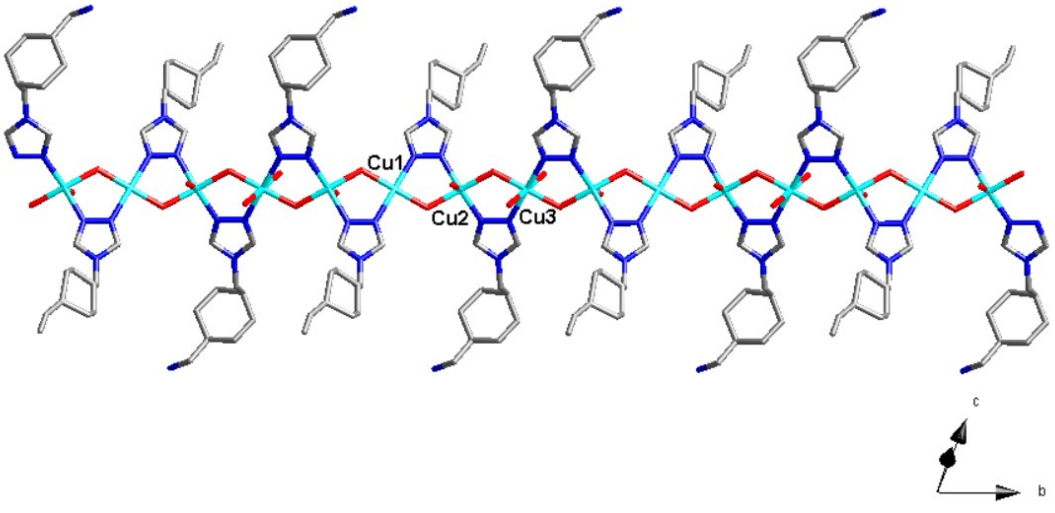

Fig. S2. The 1D metal-organic chain of compound **2** with ligands mct and ctcm in the form of AABB.

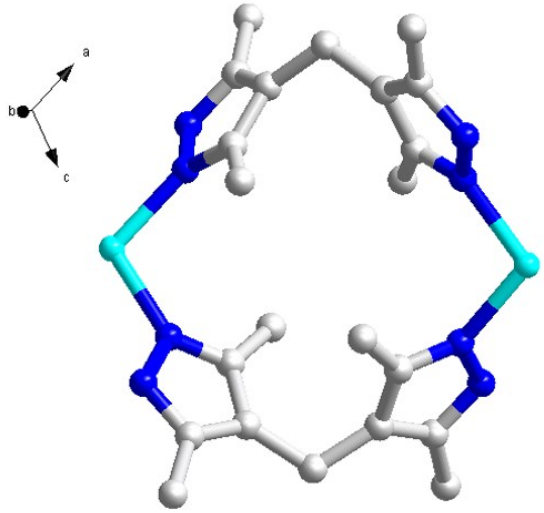

Fig. S3. The bi-nuclear cycle $\{Co_2(H_2bdpm)_2\}^{4+}$ in compound **5**.

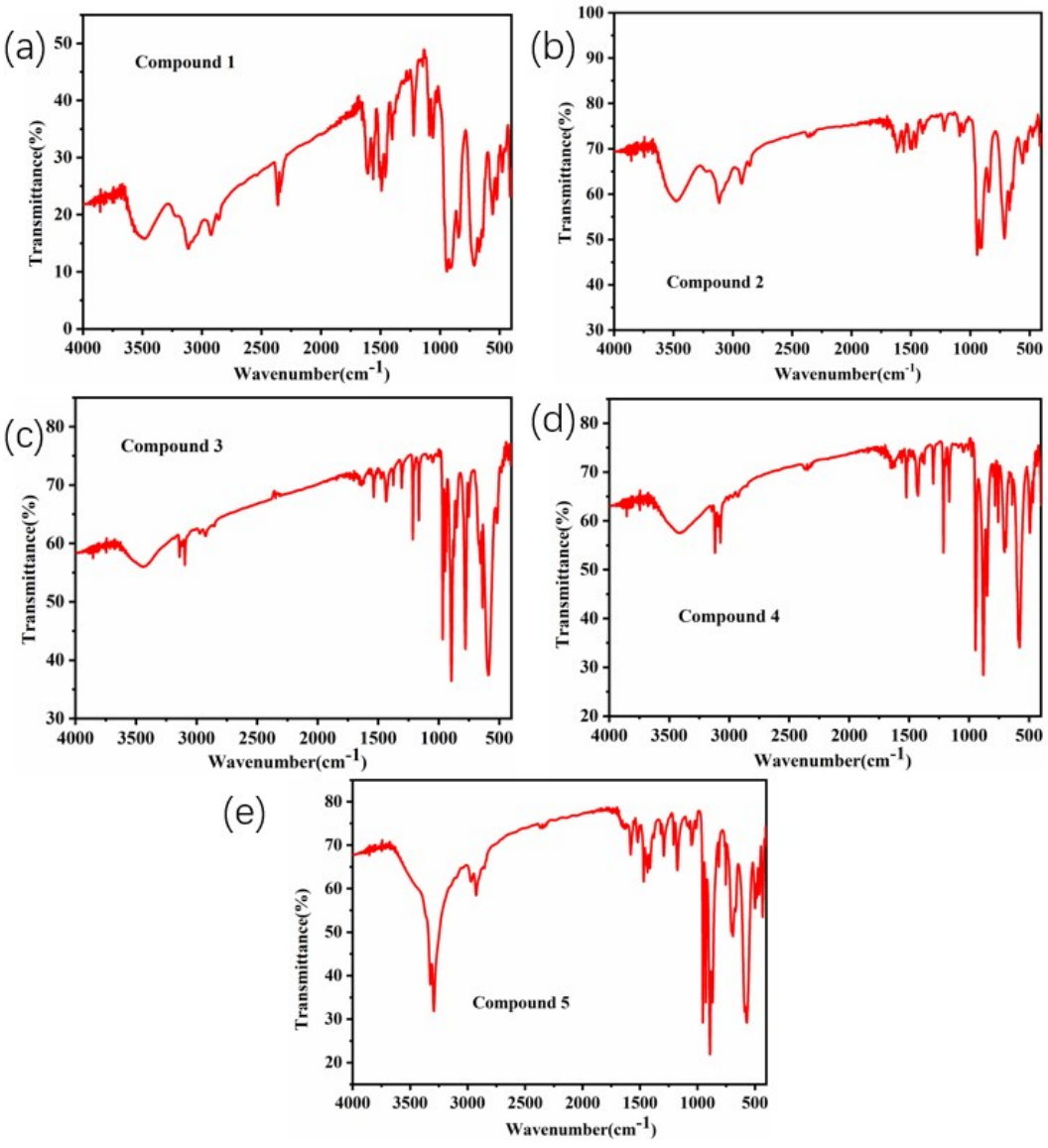

Fig. S4. The IR spectra of compounds **1**–**5**.

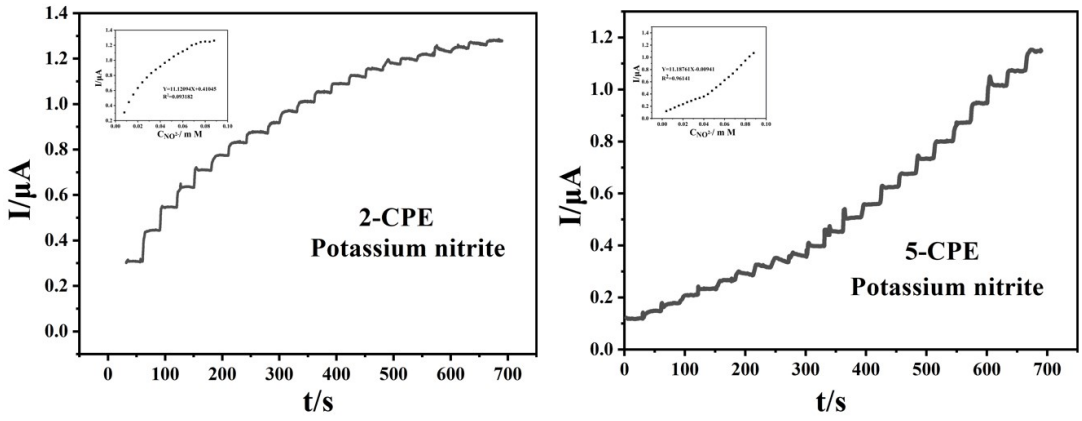

Fig. S5. Amperometric response for the **2–** and **5**−CPEs on successive addition of 0.1 mM NO_2^- to 0.1 M H_2SO_4 + 0.5 M Na_2SO_4 aqueous solution (The inset: the steady-state calibration curve for current versus NO_2^- concentration. Applied potential: 240 mV for **2**–CPE and 200 mV for **5**–CPE).

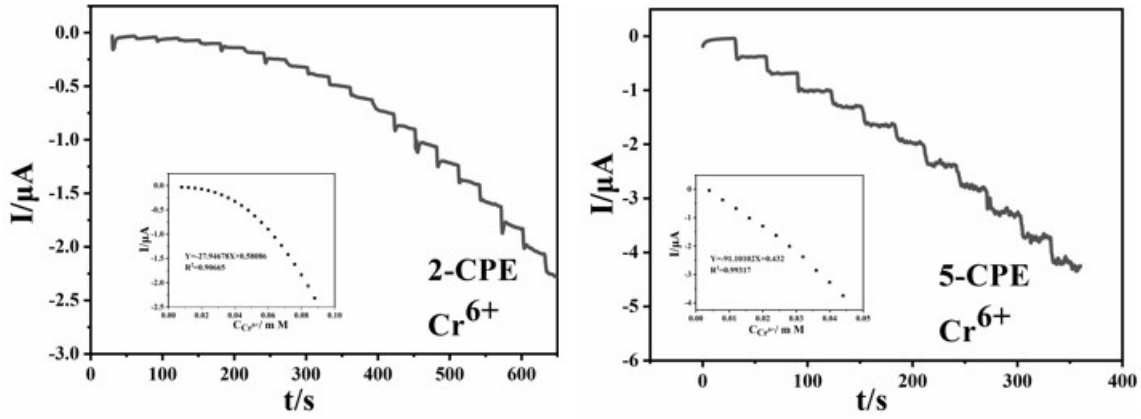

Fig. S6. Amperometric response for the **2–** and **5**−CPEs on successive addition of 0.1 mM Cr(VI) to 0.1 M H_2SO_4 + 0.5 M Na_2SO_4 aqueous solution (The inset: the steady-state calibration curve for current versus Cr(VI) concentration. Applied potential: 240 mV for **2**–CPE and 200 mV for **5**–CPE).

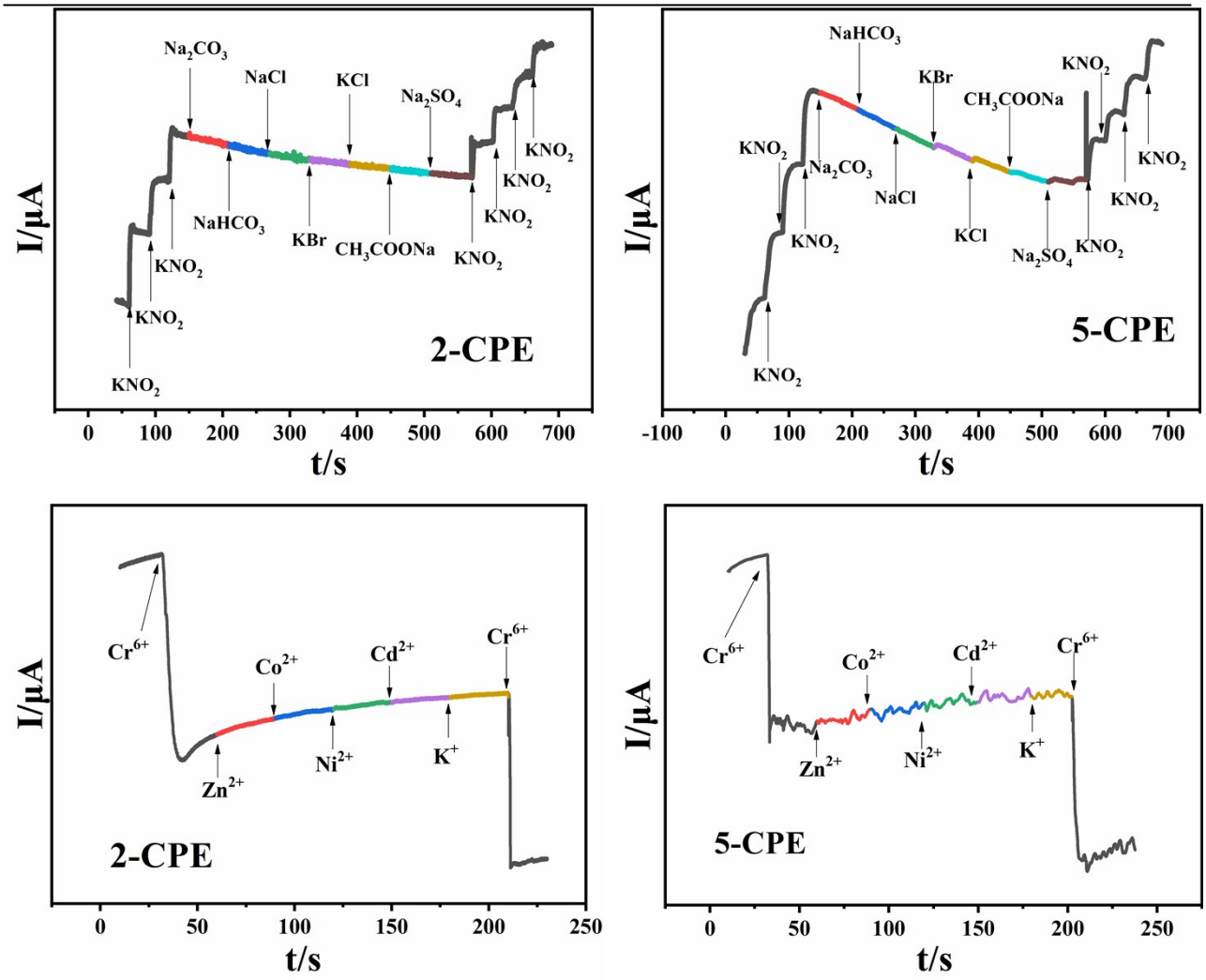

Fig. S7. Amperometric current responses of **2**– and **5**–CPEs to NO_2^- and Cr(VI) in aqueous solution upon addition of various inorganic salts.

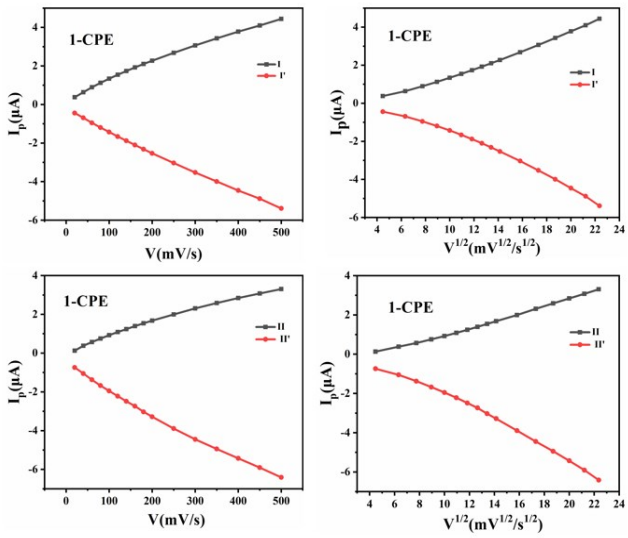

Fig. S8. Plots of the anodic and the cathodic peak I-I′ and II–II′ current against υ and $\upsilon^{1/2}$ of **1**–CPE.

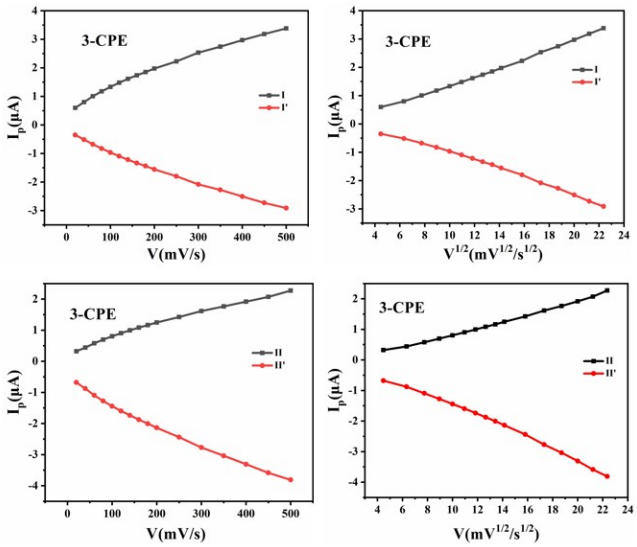

Fig. S9. Plots of the anodic and the cathodic peak I-I′ and II–II′ current against υ and $υ^{1/2}$ of **3**–CPE.

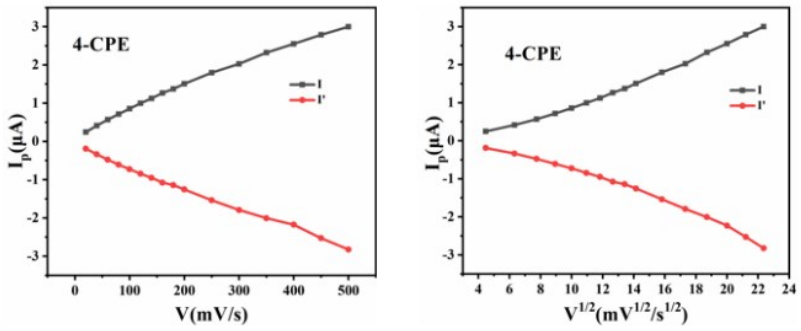

Fig. S10. Plots of the anodic and the cathodic peak I-I′ current against υ and $υ^{1/2}$ of **4**–CPE.

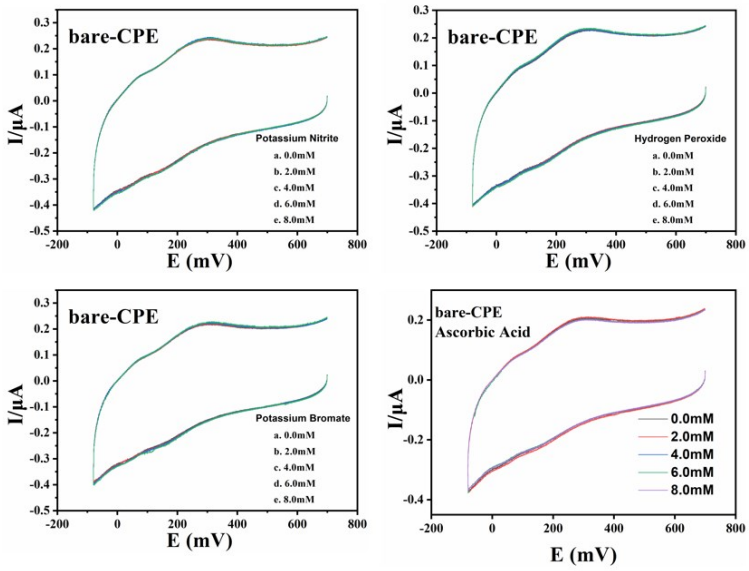

Fig. S11. Cyclic voltammograms of the bare-CPEs in 0.1 M H_2SO_4 + 0.5 M Na_2SO_4 aqueous solution

containing 0-8.0 mM H_2O_2/KNO_2/ $KBrO_3$/AA. Scan rate: 250 mV·s^{-1}.

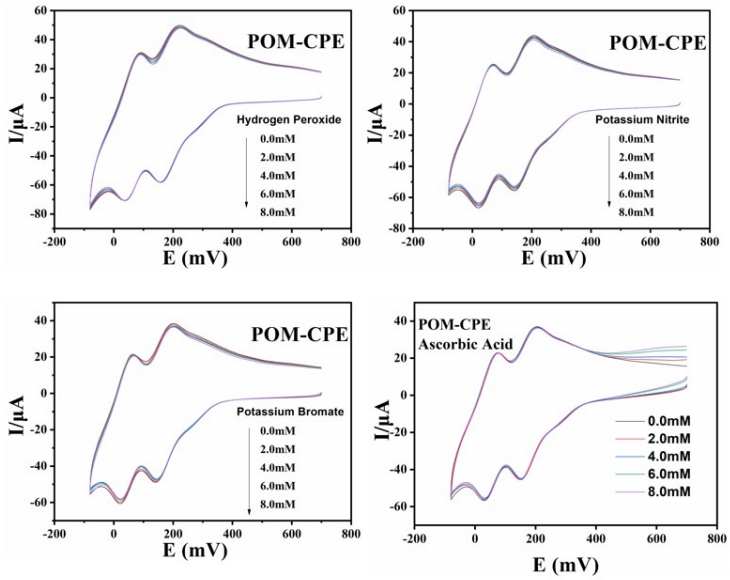

Fig. S12. Cyclic voltammograms of the POM-CPEs in 0.1 M H_2SO_4 + 0.5 M Na_2SO_4 aqueous solution containing 0-8.0 mM H_2O_2/KNO_2/ $KBrO_3$/AA. Scan rate: 250 mV·s^{-1}.

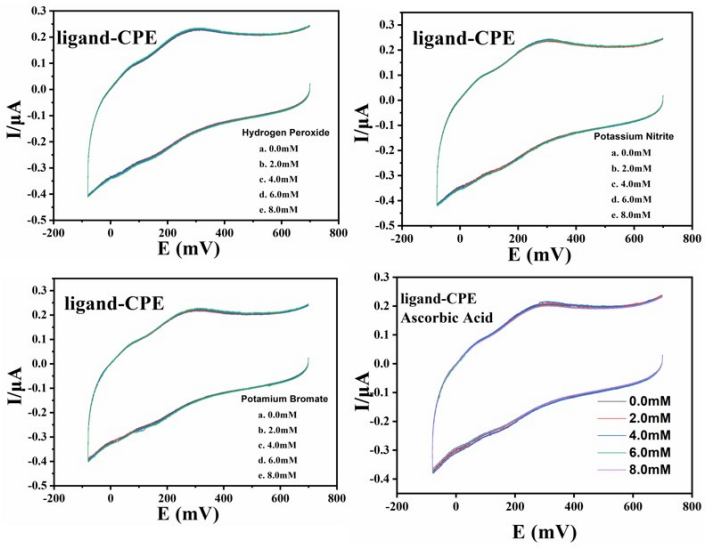

Fig. S13. Cyclic voltammograms of the ligand-CPEs in 0.1 M H_2SO_4 + 0.5 M Na_2SO_4 aqueous solution containing 0-8.0 mM H_2O_2/KNO_2/ $KBrO_3$/AA. Scan rate: 250 mV·s^{-1}.

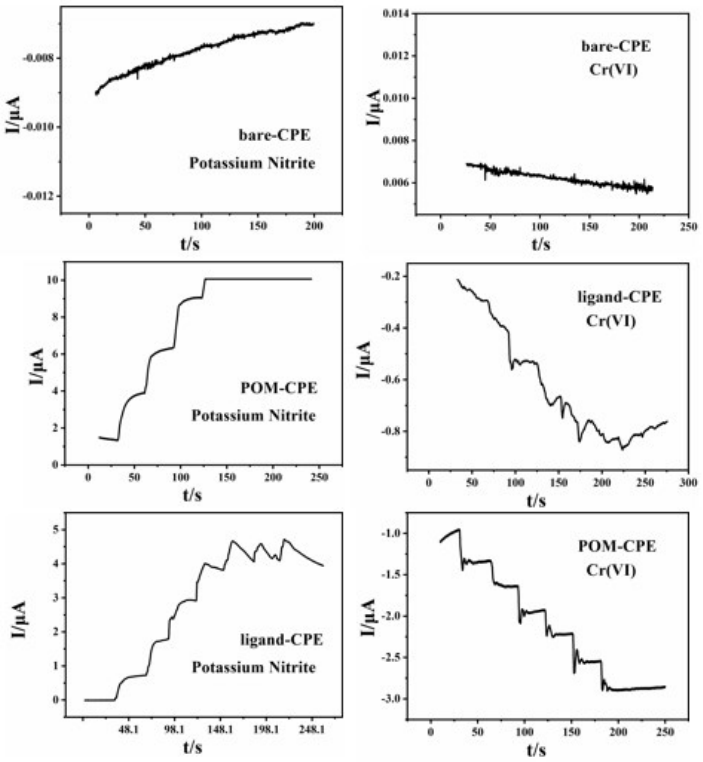

Fig. S14. Amperometric response for the bare, POM and ligand−CPEs on successive addition of 0.1 mM NO_2^- and Cr^{6+} to 0.1 M H_2SO_4 + 0.5 M Na_2SO_4 aqueous solution (Applied potential: 140 mV for bare, POM, ligand–CPEs).

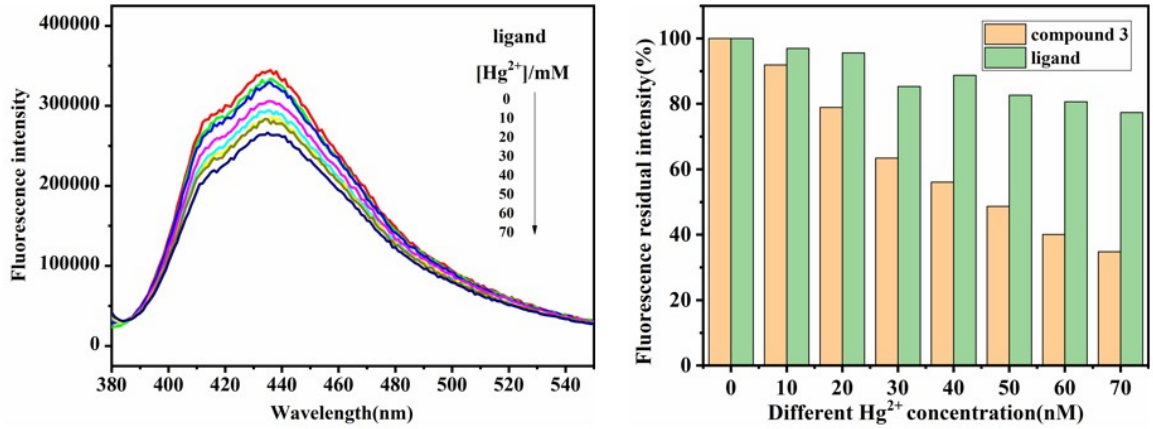

Fig. S15. (a) Fluorescence intensity of ligand suspension with gradually increased Hg^{2+}; (b) Bar diagram to show fluorescence residual intensity of compound **3** and ligand suspension upon addition of different Hg^{2+} concentrations.

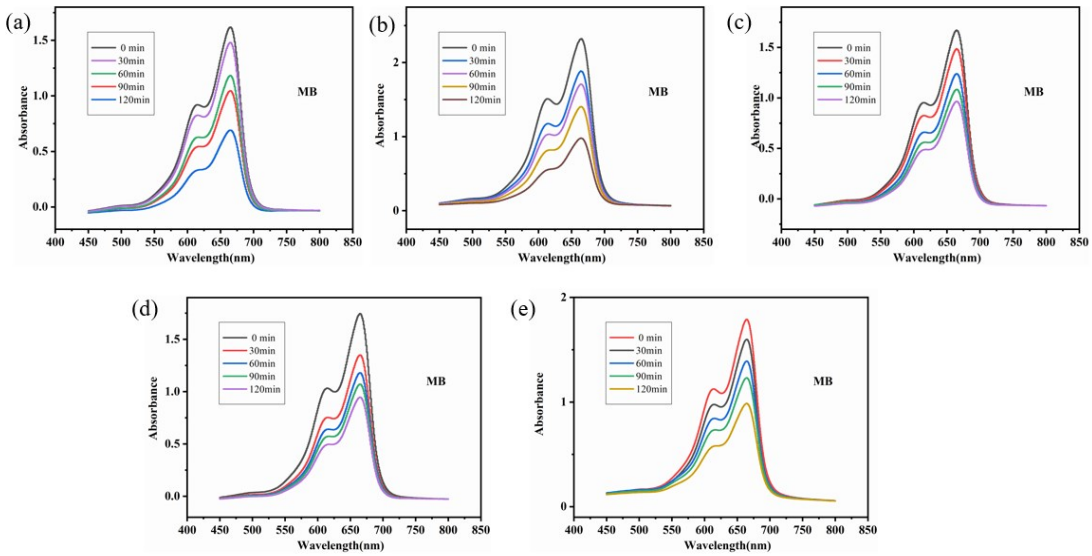

Fig. S16. (a)–(e) Absorption spectra of the MB solutions during the decomposition reaction under UV irradiation with the presence of compounds **1–5**.

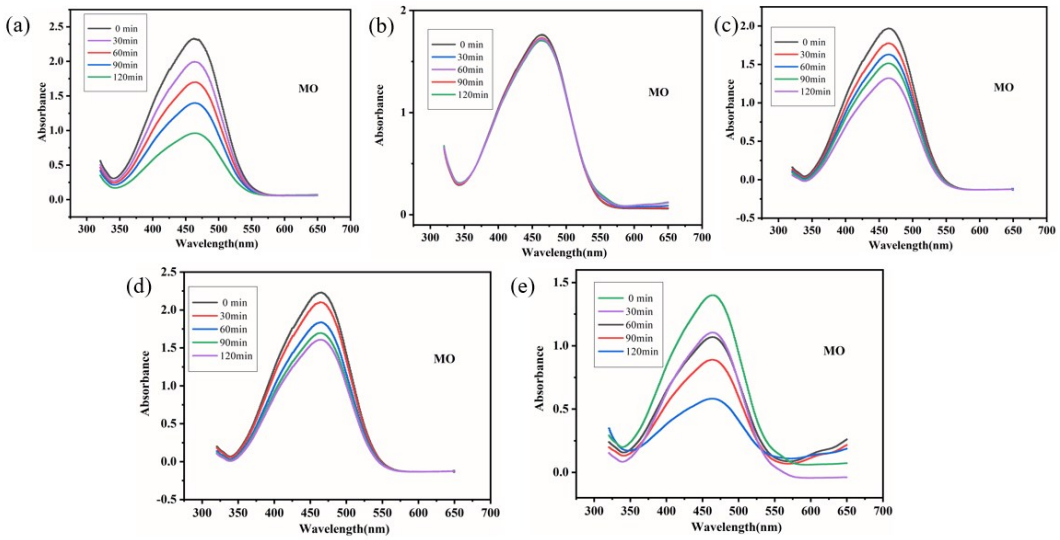

Fig. S17. (a)–(e) Absorption spectra of the MO solutions during the decomposition reaction under UV irradiation with the presence of compounds **1–5**.

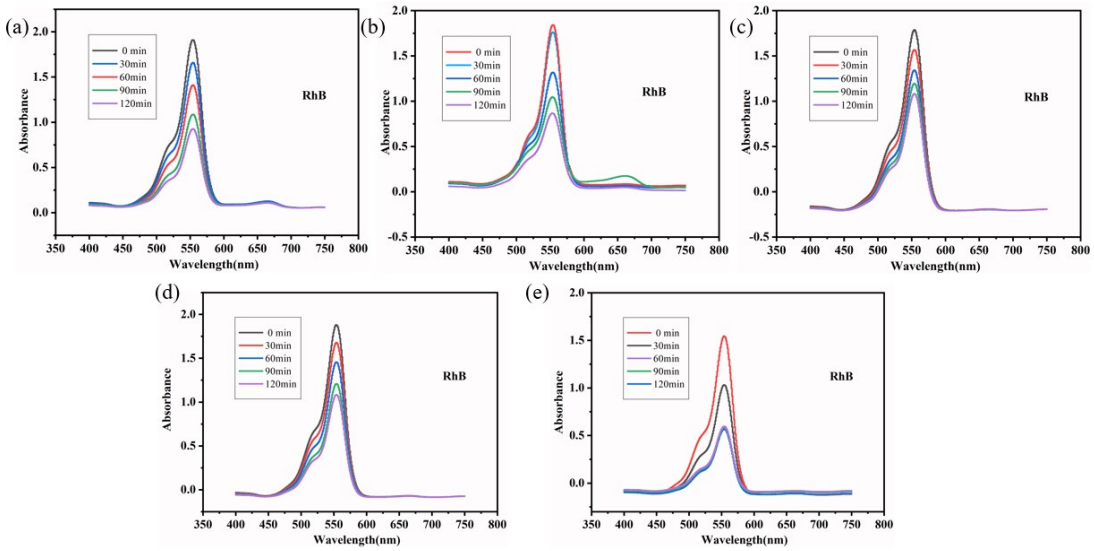

Fig. S18. (a)–(e) Absorption spectra of the RhB solutions during the decomposition reaction under UV irradiation with the presence of compounds **1–5**.

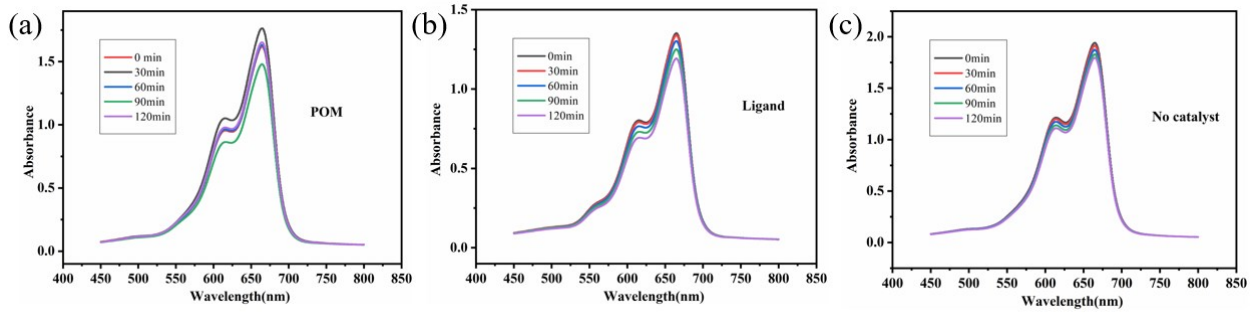

Fig. S19. (a)–(c) Absorption spectra of the MB solutions during the decomposition reaction under UV irradiation with POM, ligand and no catalyst.

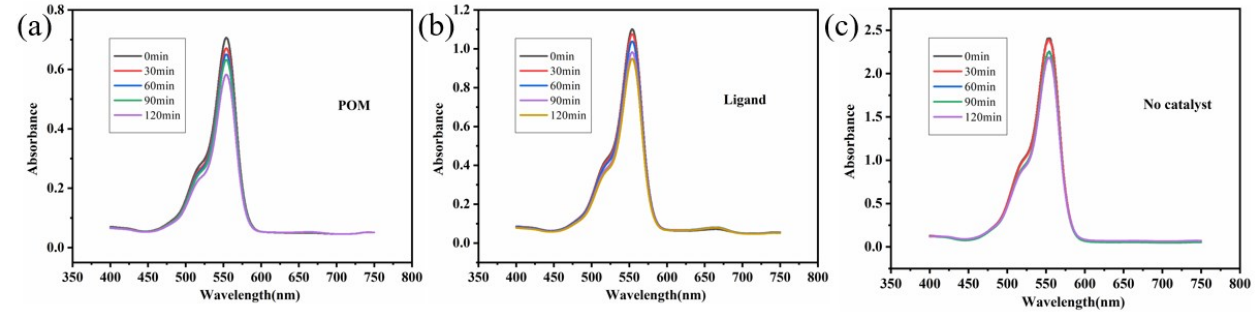

Fig. S20. (a)–(c) Absorption spectra of the Rhb solutions during the decomposition reaction under UV irradiation with POM, ligand and no catalyst.

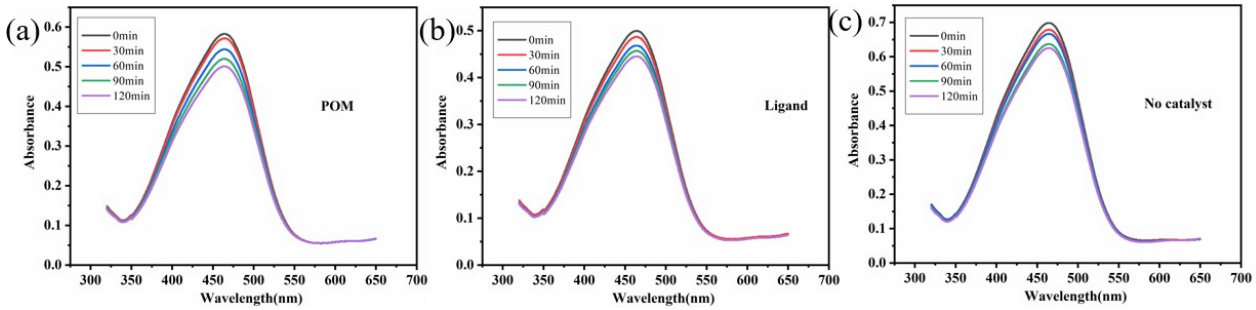

Fig. S21. (a)–(c) Absorption spectra of the MO solutions during the decomposition reaction under UV irradiation with POM, ligand and no catalyst.

Table S1. Selected bond distances (Å) and angles (°) for compounds **1–5**.

		Compound **1**	
Cu(1)-N(5)	1.909(15)	Cu(1)-N(10)	1.924(14)
Cu(1)-N(22)#3	2.029(19)	Cu(2)-N(13)	1.935(12)
Cu(2)-N(9)	1.924(13)	Cu(2)-N(21)#3	2.164(18)
Cu(3)-N(14)	1.931(12)	Cu(3)-N(1)	1.950(13)
Cu(3)-N(17)	2.007(11)	Cu(4)-N(2)	1.901(13)
Cu(4)-N(6)	1.928(14)	Cu(4)-N(18)	2.063(11)
C(11)-N(5)	1.28(2)	C(22)-N(9)	1.31(2)
C(3)-N(3)	1.44(2)	C(12)-N(6)	1.31(2)
N(19)-C(43)	1.38(3)	C(4)-C(5)	1.48(3)
N(9)-Cu(2)-N(13)	152.5(6)	N(2)-Cu(4)-N(6)	157.7(6)
N(1)-Cu(3)-N(17)	106.4(6)	N(5)-Cu(1)-N(10)	135.7(6)
C(31)-N(14)-Cu(3)	133.2(12)	N(10)-N(9)-Cu(2)	120.4(10)
C(22)-N(9)-Cu(2)	131.6(11)	N(1)-N(2)-Cu(4)	122.9(10)
C(1)-N(2)-Cu(4)	132.1(12)	N(5)-N(6)-Cu(4)	117.4(11)
		Compound **2**	
Cu(1)-O1W	1.913(5)	Cu(1)-N(6)	1.990(7)
C(8)-C(9)	1.53(2)	Cu(2)-O1W	1.916(5)
Cu(2)-O2W	1.917(5)	Cu(2)-N(1)	1.979(7)
Cu(2)-N(5) #4	1.986(7)	Cu(3)-O2W	1.912(5)

Cu(3)-N(2)	2.007 (7)	N(1)-C(11)	1.286(11)
C(1)-N(7)	1.308(12)	N(3)-C(11)	1.367(12)
N(6)-Cu(1)-O1W	91.9(2)	O1W-Cu(2)-O2W	167.4(3)
O1W-Cu(2)-N(5) #4	88.8(2)	N(1)-Cu(2)-N(5) #4	158.4(3)
O3W-Cu(3)-N(2)	86.0(5)	O2W-Cu(3)-O3W	84.6(5)

Compound **3**

Cu(1)-N(1)	2.015(5)	Cu(1)-N(2)	1.975(4)
Cu(1)-O(3)#3	2.264(4)	Cu(1)-O(6)	1.967(4)
Cu(1)-O(9)	1.913(3)	S(2)-C(7)	1.716(6)
S(2)-C(6)	1.704(8)	S(1)-C(3)	1.701(7)
S(1)-C(2)	1.710(6)	N(1)-C(7)	1.312(7)
O(9)-Cu(1)-O(6)	87.55(18)	O(9)-Cu(1)-N(1)	95.23(17)
O(9)-Cu(1)-N(2)	172.7(2)	O(6)-Cu(1)-N(1)	151.81(18)
N(2)-Cu(1)-N(1)	83.25(19)	O(2)-Cu(1)-O(3)#3	89.80(18)

Compound **4**

Co(1)-N(1)	2.111(3)	Co(1)-N(2)	2.101(3)
Co(1)-O(3)	2.090(3)	Co(1)-O(6)	2.142(3)
Co(1)-O(2)#2	2.116(2)	Co(1)-O(7)#3	2.239(2)
S(1)-C(2)	1.717(4)	S(1)-C(3)	1.702(5)
N(2)-C(5)	1.392(5)	N(2)-C(7)	1.318(5)
N(2)-Co(1)-O(6)	98.42(11)	N(2)-Co(1)-N(1)	79.20(13)
N(1)-Co(1)-O(6)	89.16(11)	O(3)-Co(1)-N(1)	171.45(11)
O(3)-Co(1)-N(2)	104.51(12)	O(3)-Co(1)-O(6)	82.70(10)

Compound **5**

Co(1)-O(2)	2.086(3)	Co(1)-O(3)	2.058(3)
Co(1)-N(2)	2.057(3)	Co(1)-O(7)#4	2.095(3)
Co(1)-O(1)#2	2.254(3)	N(2)-N(1)	1.361(5)
N(2)-Co(1)-O(2)	90.03(12)	N(2)-Co(1)-O(3)	94.55(12)
O(3)-Co(1)-O(2)	82.60(11)	O(3)-Co(1)-O(7)#4	160.17(11)

N(3)#5-Co(1)-O(7)#4	95.36(12)	N(2)-Co(1)-O(3)	94.55(12)

Symmetry codes: #2 -x,-y,-x; #3 1-x,1-y,-z; #4 2-x,1-y,-z ;#5 1-x,+y,1/2-z

Table. S2. Comparison of different amperometric sensors of NO_2^-.

Electrode material	Method	Concentration range	Detection limit	Ref.
1-CPE	CV	0.008-0.08 mM	1.4×10^{-7} M	This work
2-CPE	CV	0.008-0.088mM	5.6×10^{-7} M	This work
3-CPE	CV	0.004-0.092 mM	1.135×10^{-7} M	This work
4-CPE	CV	0.004-0.088 mM	1.264×10^{-6} M	This work
5-CPE	CV	0.004-0.088 mM	4.26×10^{-8} M	This work
CR-GO/GCE	Amperometry	0.0089-0.167 mM	1.0×10^{-6}M	**1**
RGO-MWNT	DPV	0.075–6.060 mM	2.5×10^{-5} M	**2**
TOBA/ZnP$_p$-C$_{60}$	Amperometry	0.002-0.164 mM	1.44×10^{-6} M	**3**

Table. S3. Comparison of different amperometric sensors of Cr^{6+}.

Electrode material	Method	Concentration range	Detection limit	Ref.
1-CPE	Amperometry	0.004-0.032 mM	7.4×10^{-8} M	This work
2-CPE	Amperometry	0.008-0.088 mM	2.5×10^{-7} M	This work
3-CPE	Amperometry	0.004-0.092 mM	6.5×10^{-7} M	This work

4-CPE	Amperometry	0.004-0.032 mM	7.35×10^{-6} M	This work
5-CPE	Amperometry	0.004-0.044 mM	1.03×10^{-6} M	This work
AuSPE	CV	0.01-1.6 mM	4.4×10^{-6} M	**4**
screen-printed carbon electrode	FIP response	0.001-0.316 mM	7.7×10^{-7} M	**5**
Fe_3O_4/MoS_2 composite	Amperometry	0.0005-0.328 mM	0.2×10^{-6}	**6**

1. J. P. Metters, R. O. Kadara and C. E. Banks, Electroanalytical sensing of chromium(III) and (VI) utilising gold screen printed macro electrodes, *Analyst,* 2012, **137**, 896-902.
2. F. X. Hu, S. H. Chen, C. Y. Wang, R. Yuan, D. H. Yuan and C. Wang, Study on the application of reduced graphene oxide and multiwall carbon nanotubes hybrid materials for simultaneous determination of catechol hydroquinone, p-cresol and nitrite, *Analytica Chimica Acta,* 2012, **724**, 40-46.
3. Y. Zhang, P. Chen, F. F. Wen, B. Yuan and H. G. Wang, Fe3O4 nanospheres on MoS2 nanoflake: Electrocatalysis and detection of Cr(VI) and nitrite, *Journal of Electroanalytical Chemistry,* 2016, **761**, 14-20.
4. J. P. Metters, R. O. Kadara and C. E. Banks, Electroanalytical sensing of chromium(III) and (VI) utilising gold screen printed macro electrodes, *Analyst,* 2012, **137**, 896-902.
5. R. A. Sanchez-Moreno, M[a]. J. Gismera, M[a]. T. Sevilla and J. R. Procopio, Potentiometric Screen-Printed Bisensor for Simultaneous Determination of Chromium(III) and Chromium(VI), *Electroanalysis,* 2011, **23**, 287-294.
6. Y. Zhang, P. Chen, F. F. Wen, B. Yuan and H. G. Wang, Fe_3O_4 nanospheres on MoS_2 nanoflake: Electrocatalysis and detection of Cr(VI) and nitrite, *Journal of Electroanalytical Chemistry,* 2016, **761**, 14-20.